# Förster Excitation Energy Transfer in Peridinin-Chlorophyll-*a*-Protein

Foske J. Kleima,* Eckhard Hofmann,[†] Bas Gobets,* Ivo H. M. van Stokkum,* Rienk van Grondelle,*
Kay Diederichs,[†] and Herbert van Amerongen*

*Faculty of Sciences, Division of Physics and Astronomy and Institute for Condensed Matter Physics and Spectroscopy, Vrije Universiteit, 1081 HV Amsterdam, the Netherlands, and [†]Fakultät für Biologie, Universität Konstanz, D-78457 Konstanz, Germany

ABSTRACT   Time-resolved fluorescence anisotropy spectroscopy has been used to study the chlorophyll *a* (Chl *a*) to Chl *a* excitation energy transfer in the water-soluble peridinin–chlorophyll *a*–protein (PCP) of the dinoflagellate *Amphidinium carterae*. Monomeric PCP binds eight peridinins and two Chl *a*. The trimeric structure of PCP, resolved at 2 Å (Hofmann et al., 1996, *Science.* 272:1788–1791), allows accurate calculations of energy transfer times by use of the Förster equation. The anisotropy decay time constants of 6.8 ± 0.8 ps ($\tau_1$) and 350 ± 15 ps ($\tau_2$) are respectively assigned to intra- and intermonomeric excitation equilibration times. Using the ratio $\tau_1/\tau_2$ and the amplitude of the anisotropy, the best fit of the experimental data is achieved when the $Q_y$ transition dipole moment is rotated by 2–7° with respect to the *y* axis in the plane of the Chl *a* molecule. In contrast to the conclusion of Moog et al. (1984, *Biochemistry.* 23:1564–1571) that the refractive index (*n*) in the Förster equation should be equal to that of the solvent, *n* can be estimated to be 1.6 ± 0.1, which is larger than that of the solvent (water). Based on our observations we predict that the relatively slow intermonomeric energy transfer in vivo is overruled by faster energy transfer from a PCP monomer to, e.g., the light-harvesting *a/c* complex.

## INTRODUCTION

The dinoflagellate *Amphidinium carterae* contains a water-soluble peridinin–chlorophyll *a*–protein (PCP) that acts as an accessory photosynthetic light-harvesting pigment-protein complex. The complex transfers its excitation energy to photosystem II (PSII) (Mimuro et al., 1990). However, it is not known whether this transfer is directly to the PSII antenna complex (Knoetzel and Rensing, 1990) or via the membrane-bound light-harvesting complex (LHC*a/c*) (Hofmann et al., 1996). The main light-absorbing pigment of PCP is peridinin, which absorbs in the 470–550-nm region. Besides peridinin the complex binds chlorophyll *a* (Chl *a*). The pigments are bound to a 30.2-kDa protein and are organized into two clusters of pigments, each consisting of four peridinins and one Chl *a* (see, e.g., Carbonera and Giacometti, 1995). Singlet energy transfer from peridinin to Chl *a* occurs with an efficiency close to 100% (Song et al., 1976; Koka and Song, 1977) on a time scale of a few picoseconds (Bautista et al., 1999; Akimoto et al., 1996).

Recently, the crystal structure of PCP was resolved at a resolution of 2.0 Å (Hofmann et al., 1996), revealing a trimeric organization of the complex. The protein mainly has an *α*-helical structure and forms a cavity in which the two pigment clusters are located (Hofmann et al., 1996). The distance between the centers of the two Chl *a* in one monomer is 17.4 Å, whereas the distance between two Chl *a* bound to different monomers ranges from 40 to 54 Å (Hofmann et al., 1996). All peridinins are organized in pairs with a closest distance to each other of 4 Å, and they are in van der Waals contact with the Chl *a*. The resolution is high enough to distinguish the *x* and *y* axes of the Chl *a* molecules, allowing a definition of the orientation of the $Q_y$ transition dipole moment within the molecular frame of Chl *a* in PCP. Therefore, PCP forms an excellent system for the study of the Chl *a* to Chl *a* excitation energy transfer in a relatively simple pigment-protein complex and to test whether it can be modeled using the Förster equation (Förster, 1965).

A detailed test of the Förster equation was conducted before by Debreczeny et al. (1995a,b) on another pigment-protein complex with a known crystal structure (Schirmer et al., 1987; Duerring et al., 1991), namely monomeric and trimeric C-phycocyanin (CPC) from *Synechococcus sp.* The pigments responsible for light harvesting in this complex are open-chain tetrapyrrole chromophores (also called phycocyanobilins). The three pigments bound to each monomer are relatively far apart; however, in the trimer two pigments bound to different monomers are relatively close. The energy transfer processes in the monomeric and trimeric complexes were studied using time-resolved polarized fluorescence experiments by Gillbro et al. (1993) and Debreczeny et al. (1995a,b). It was concluded by Debreczeny et al. (1995a,b, 1993) that the equilibration rates are in good correspondence with those that can be calculated using the Förster equation, with the refractive index (which is an important parameter in this equation) being that of the solvent, in this case water ($n = 1.33$). It was argued before by Moog et al. (1984) that when the Förster equation is applied to protein-chromophore complexes, the refractive index of the solvent should be used.

In the present study we focus on the Chl *a* to Chl *a* excitation energy transfer in PCP, using time-resolved fluorescence anisotropy spectroscopy. We show that the ex-

perimental equilibration rates and the rates calculated using the Förster equation are in reasonable agreement when the Chl $a$ $Q_y$ transition dipole moments are oriented along the molecular $y$ axis. However, we find a better match when these dipole moments are rotated by 2–7°. In contrast to the conclusion by Moog et al. (1984), in the case of PCP the refractive index in the Förster equation is larger than the refractive index of the solvent, which is water, and it is estimated to be 1.60 ± 0.1.

## MATERIALS AND METHODS

### Sample preparation

PCP was purified according to the method described by Hofmann et al. (1996). Measurements were performed in a buffer containing 25 mM Tris-HCl (pH 7.5), 3 mM $NaN_3$, and 2 mM KCl.

### Absorption and steady-state fluorescence emission spectroscopy

The absorption spectra were recorded on a Cary 219 spectrophotometer, using an optical bandwidth of 1 nm. Steady-state fluorescence emission spectra were recorded using a CCD camera (Chromex Chromcam 1) via a ½ m spectrograph (Chromex 500IS). Excitation light was provided by a tungsten-halogen lamp via a band-pass filter at 475 nm with a full width at half-maximum (FWHM) of 15 nm. The fluorescence emission spectra were corrected for the wavelength sensitivity of the detection system.

### Time-resolved fluorescence anisotropy

The optical density of the sample was 0.2/cm at the excitation wavelength (660 nm) and 0.6/cm in the absorbance maximum at 670 nm. The sample was kept at room temperature in a spinning cell (light path of 0.22 cm, diameter 10 cm, frequency 15 Hz) refreshing the sample every few shots. The spinning cell was placed at an angle of 45° with respect to the excitation light. Comparison of the OD spectrum of the sample before and after the experiment showed that less than 10% of the absorption was lost after an experiment with a duration of several hours. The spectrum essentially did not change. Two independent series of experiments were performed.

Pulses of 150–200 fs at 660 nm with a FWHM of 7 nm were generated at a 100-kHz repetition rate, using a Ti:sapphire based oscillator (Coherent MIRA), a regenerative amplifier (Coherent REGA), and a double-pass optical parametric amplifier (OPA-9400; Coherent). The intensity was adjusted so that less than 1 photon/20 trimeric complexes was absorbed per laser shot. The polarization of the excitation light was adjusted with a Soleil Babinet compensator.

The fluorescence was detected at a right angle with respect to the excitation beam through a sheet polarizer, using a Hamamatsu C5680 synchroscan streak camera equipped with a Chromex 250IS spectrograph (4-nm spectral resolution, 3-ps time response). The streak images were recorded on a Hamamatsu C4880 CCD camera, which was cooled to −55°C. Streak images were recorded on two different time scales (200 ps and 2200 ps full range) and over a wavelength range of 315 nm, with the detection polarizer oriented alternately parallel and perpendicular to the vertically polarized excitation light. The polarization dependence of the sensitivity of the apparatus was measured by recording streak images, using horizontally polarized excitation light, with the polarizer in the detection branch oriented both horizontally and vertically, and is expressed in the so-called $g$ factor.

### Global analysis

The measurements on both time scales and with both polarizations were fitted simultaneously, using a global analysis program (van Stokkum et al., 1994) for the wavelength region in which no scattering of the exciting laser light was present. The two independent series of experiments were fitted separately. Included in the fitting procedure is the signal that is detected in the back sweep of the streak camera, which is 6–8 ns after the excitation pulse. The experimentally determined $g$ factor was introduced into the fitting procedure. In the model an initial anisotropy of 0.4 is assumed. The amplitudes of the fitted kinetics are rather sensitive to small variations in the $g$ factor; however, the variation in the corresponding time constants is limited. For both data sets we have estimated the error margins for the amplitudes by examining the consequences of small variations in the $g$ factor.

## RESULTS

### Absorption and fluorescence

In Fig. 1 the absorption (*solid line*) and fluorescence emission (*dashed line*) spectra of PCP at room temperature are shown. The inset shows the overall absorption spectrum of PCP at room temperature. The absorption band at 670 nm is due to the $Q_y$ band of Chl $a$ and has a FWHM of 14 nm. The absorption in the 450–600-nm region is due to peridinin, and the peak at 430 nm is due to the Soret band of Chl $a$. The spectrum is very similar to the absorption spectra of PCP reported before (Koka and Song, 1977; Carbonera et al., 1996). In the time-resolved fluorescence emission experiment the sample was excited at 660 nm (*thick vertical line* in Fig. 1), and the anisotropy was calculated from the fluorescence detected between 675 and 700 nm. The anisotropy decay was independent of the detection wavelength. The absorption and fluorescence emission spectra shown
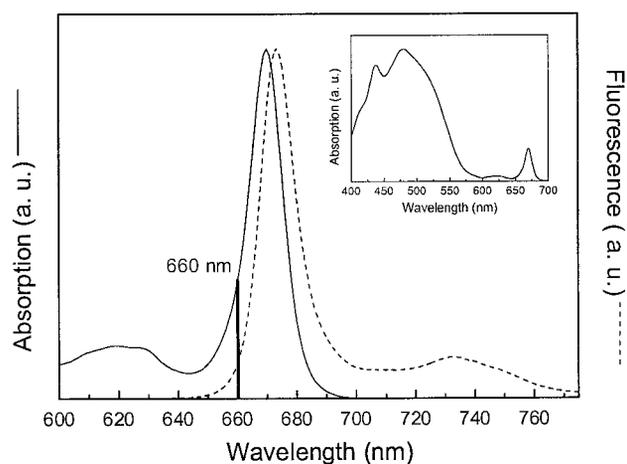


FIGURE 1 Absorption spectrum (*solid line*) and fluorescence emission spectrum (*dashed line*) of PCP at room temperature (excitation at 475 nm). The excitation wavelength (= 660 nm) used for the time-resolved anisotropy measurement is indicated by a thick solid line. The inset shows the overall absorption spectrum of PCP at room temperature.

here were used for the calculation of the Förster overlap integral (see Appendix 2).

## Time-resolved fluorescence anisotropy

In Fig. 2 the $F_{/\!/}(t)$ and $F_{\perp}(t)$ components (polarization of the detection being parallel and perpendicular to the vertical polarization of the excitation light, respectively) of the fluorescence emission spectra are plotted on a linear-logarithmic time scale for the 200-ps window (Fig. 2 $A$) and for the 2200-ps time window (Fig. 2 $B$). The detection wavelength of these traces was 675 nm. At detection wavelengths shorter than 675 nm, scattering of the excitation light contributes at time scales on the order of the instrument response. The anisotropy was independent of the detection wavelength; therefore the 675–700-nm region was fitted using a global analysis routine (van Stokkum et al., 1994). The solid lines in Fig. 2 show the result of a simultaneous fit of the $F_{/\!/}(t)$ and $F_{\perp}(t)$ components in the two time domains. In the fit procedure the anisotropy at $t = 0$ was fixed at 0.4. Two decay time constants were needed to fit the decay of the anisotropy $r(t)$:

$$r(t) = A_1 e^{-t/\tau_1} + A_2 e^{-t/\tau_2} + r_{\infty} = 0.24 e^{-t/(6.8 \pm 0.8)}$$
$$+ 0.05 e^{-t/(350 \pm 15)} + 0.11 \quad (1)$$

The two depolarization times $\tau_1$ and $\tau_2$ are tentatively interpreted as intra- and intermonomeric equilibration times,
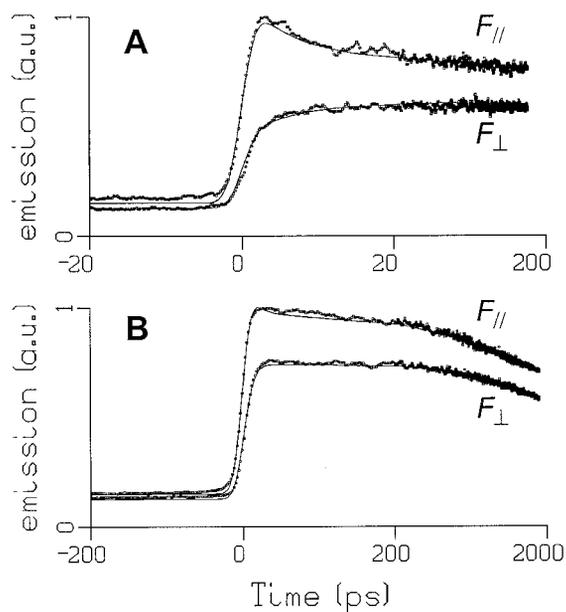
respectively. The error margins are estimated on the basis of the fits of two independent series of experiments. The estimated error margin of the amplitude of the fast process ($A_1$) is 0.24 $\pm$ 0.02. The amplitude of the 350 $\pm$ 15-ps process could be estimated very accurately to be 0.05, and the fitted amplitude of the residual anisotropy is anticorrelated to the fitted amplitude of the fast process. Therefore, the amplitude of the residual anisotropy ($r_{\infty}$) is 0.11 $\pm$ 0.02. On the time scale of the fastest depolarization process hardly any depolarization due to the slower process takes place. The anisotropy "after" the fast depolarization process ($r_1$) can be defined as $r_1 = 0.4 - A_1 = 0.16 \pm 0.02$.

Because the experiment is performed in water, one might expect a third depolarization time constant caused by the rotational motion of the PCP complex. The rotational depolarization time was reported to be 33 ns (Koka and Song, 1977). On the basis of the known size of the complex one can calculate that the rotational depolarization time (Cantor and Schimmel, 1980), is $\sim$48 ns for the PCP trimer and $\sim$16 ns for the monomer. Addition of an extra component with a depolarization time constant of 16–48 ns in the global analysis procedure did not lead to an improvement of the fit, and therefore the rotational depolarization is negligible.

The isotropic fluorescence decay time constant was estimated to be $\sim$4.2 ns, which is in reasonable agreement with the fluorescence lifetime of 4.6 ns reported by Koka and Song (1977).

## DISCUSSION

### Calculation of Förster energy transfer rates based on the structure of PCP

For the application of the Förster equation two prerequisites should be fulfilled: 1) the dipole interaction approach should be justified and 2) the excitonic coupling between the pigments should be weak. In the case of PCP, the center-to-center distance between the interacting pigments is at least 17 Å, significantly larger than the conjugated part of the porphyrin, so that the dipole-dipole approximation is justified. The second constraint quantitatively implies that the coupling between the pigments is smaller than the homogeneous width of the absorption bands. The Chl $a$ $Q_y$ band of PCP has a width of 300 cm$^{-1}$, and the coupling between two Chl $a$ in a PCP monomer is on the order of 10 cm$^{-1}$ (Kleima, 1999), so the second condition is also fulfilled.

On the basis of the crystal structure of PCP, the excitation energy transfer rates can now be calculated using the Förster equation (Förster, 1965):

$$k_{DA} = \frac{\kappa^2}{R^6} \cdot \frac{k_r^D}{n^4} \cdot I = \frac{\kappa^2}{R^6} \cdot C \quad (2)$$

FIGURE 2 Time traces of the $F_{/\!/}(t)$ and $F_{\perp}(t)$ components of the fluorescence decay spectrum of 200 ps ($A$) and 2200 ps ($B$) time domains measured at room temperature, plotted with the result of the fit (*solid line*). The detection wavelength is 675 nm. Note that the time base is linear around time zero (the location of the maximum of the instrument response) and logarithmic in the range 20–200 ps ($A$) or 200–2000 ps ($B$).

with

$$I = 8.8 \times 10^{17} \cdot \int \frac{\epsilon_A(\tilde{\nu}) \cdot f_D(\tilde{\nu})}{\tilde{\nu}^4} \, d\tilde{\nu} \qquad (3)$$

Here $k_{DA}$ (ps$^{-1}$) is the rate of transfer from donor (D) to acceptor (A), $\kappa$ is an orientation factor which is given below, $n$ is the refractive index, $R$ is the distance between the centers of the interacting pigments in nm, and $k_r^D$ is the radiative rate of the donor molecule (ps$^{-1}$). The integral reflects the overlap between the fluorescence spectrum of the donor normalized to area unity and the absorption spectrum of the acceptor scaled to the value of the extinction coefficient (M$^{-1} \cdot$ cm$^{-1}$) in the absorption maximum, both on a frequency scale (cm$^{-1}$). The orientation factor $\kappa$ is given by

$$\kappa = (\hat{\mu}_1 \cdot \hat{\mu}_2) - 3(\hat{\mu}_1 \cdot \hat{r}_{12})(\hat{\mu}_2 \cdot \hat{r}_{12}) \qquad (4)$$

where $\hat{\mu}_1$ and $\hat{\mu}_2$ are the normalized transition dipole moment vectors and $\hat{r}_{12}$ is the normalized vector between the centers of pigments 1 (donor) and 2 (acceptor). The center of the Chl $a$ molecule is taken to be the center of gravity of the four nitrogen atoms in the molecular structure of Chl $a$ (see Fig. 3, *inset*). In the literature one often encounters the Förster radius ($R_0$), which is related to $C$ via $R_0^6 = \kappa^2 \cdot C/k_r^D$.

In Fig. 3 the positions of the six Chl $a$ molecules in trimeric PCP are shown (Hofmann et al., 1996). Pigments 1 and 2 are the interacting pigments in a monomer. On the basis of the trimeric structure, two energy equilibration processes can be expected: within the monomer and within the trimer, respectively. From linear dichroism and absorp-

tion spectroscopy experiments at room temperature (Kleima, 1999) it is concluded that the two Chl $a$ molecules that are bound per monomeric unit are essentially isoenergetic, which is reasonable because the two pigments are located in very similar environments.

Because the pigments are isoenergetic at room temperature, the intramonomeric equilibration rate ($k_{eqM}$) is twice the excitation energy transfer rate ($k_{eqM} = k_{12} + k_{21} = 2k_{12} = 1/\tau_{eqM}$, where $k_{nm}$ is the transfer rate from pigment $n$ to pigment $m$ and $\tau_{eqM}$ is the time constant for equilibration within the monomer). The intermonomeric equilibration rate ($k_{eqT}$) is calculated as follows:

$$k_{eqT} = 3k_{12 \to 34} = 3[0.5(k_{13} + k_{14}) + 0.5(k_{23} + k_{24})] = 1/\tau_{eqT} \qquad (5)$$

The indices refer to the pigments as shown in Fig. 3, and $\tau_{eqT}$ is the time constant for equilibration within the trimer. Because the equilibration within the monomer is fast, the transfer rate from monomer 12 to monomer 34 ($k_{12 \to 34}$) is the sum of the average transfer rates from, respectively, pigment 1 to pigments 3 and 4 and from pigment 2 to pigments 3 and 4. The equilibration rate within a trimer is three times the rate for transfer between two monomeric subunits (see, e.g., Causgrove et al., 1988). We stress that the ratio of the inter- and intramonomeric equilibration times is independent of the radiative lifetime, the refractive index, and the overlap integral, when it is assumed that these are the same for the two equilibration processes. This is a reasonable assumption because the surroundings of the Chl $a$ are very similar.



FIGURE 3   Organization of Chl $a$ in PCP. Chl $a$ 1 and 2 belong to one monomer. The arrows indicate transition dipole moments. The $r_{nm}$ show the distances between the different pairs of Chl $a$. The inset shows the structure of Chl $a$, the orientation of the $Q_y$ transition dipole moment, and the definition of $\alpha$, which is the angle between the $x$ axis and the $Q_y$ transition dipole moment. Note that the transition dipole moment is oriented parallel to the plane of the Chl $a$ molecule.
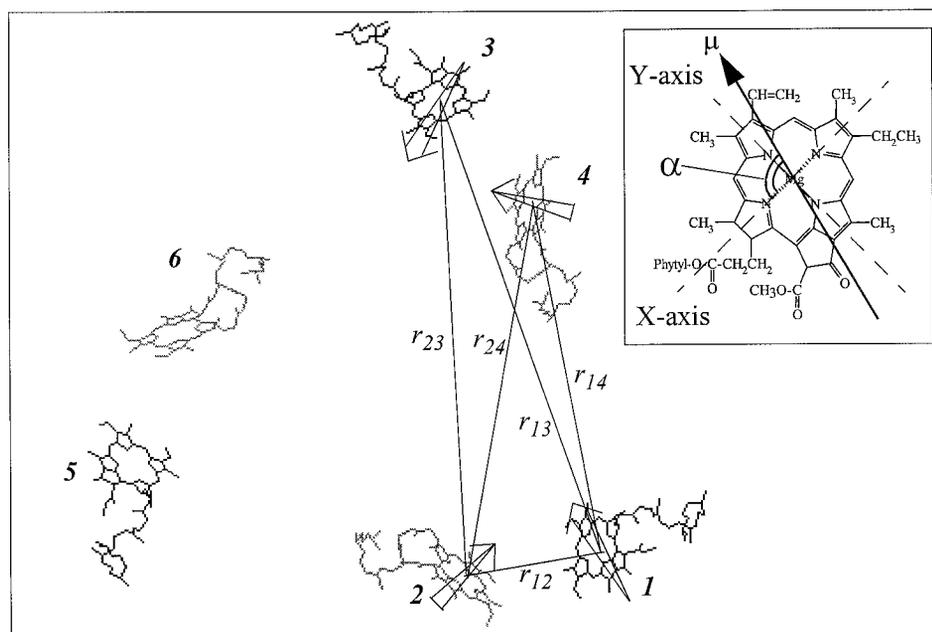
## Detailed comparison of experimentally determined and calculated transfer rates

To discuss the transfer processes in terms of the Förster equation in detail, accurate knowledge of the $Q_y$ transition dipole moment within the porphyrin plane is required. To a first approximation the dipole is often taken to be along the $y$ axis (see Fig. 3), but this is not entirely correct (see, e.g., van Zandvoort et al., 1995, and Appendix 1). In Fig. 3 the angle $\alpha$ is defined, which corresponds to the angle between the $Q_y$ transition dipole moment and the $x$ axis of the molecular frame of Chl $a$. (Note that the $y$ axis corresponds to the NB-ND axis of the Chl $a$ molecule, whereas the $x$ axis is perpendicular to the $y$ axis). Assuming that the preparation exclusively contains trimers, there are three experimentally determined parameters available that depend on the choice of $\alpha$, which will be discussed below: 1) the amount of anisotropy ($r_1$) that remains after equilibration within the monomer, 2) the residual anisotropy ($r_\infty$) that remains after equilibration within the trimer, and 3) the ratio $\tau_1/\tau_2$ of the equilibration within the monomer and trimer, respectively. However, a complicating factor is the fact that the preparation does not only contain trimers. Using ultracentrifugation techniques, it was shown that the percentage of PCP trimers present in a preparation depends on the PCP concentration, and, at the concentration applied in our experiments, one expects the presence of both monomers and trimers (Hofmann et al., unpublished results). Because biochemical separation of the monomers and trimers affects the monomer/ trimer equilibrium, the exact percentages of monomers and trimers at a certain initial PCP concentration are hard to give. As a consequence, $r_1$ provides the most unambiguous information about $\alpha$ because this term is independent of the state of oligomerization (assuming that the relative orientations of the Chl molecules within the monomer are the same in all cases).

The expected anisotropy after equilibration within the monomer ($r_{eqM}$) can be calculated using $r_{eqM} = 0.5(0.4 + r_{1\rightarrow2})$ with $r_{1\rightarrow2} = 0.2 \, (3\cos^2\phi_{12} - 1)$, where $r_{1\rightarrow2}$ is the anisotropy after 100% energy transfer from pigment 1 to pigment 2 and $\phi_{12}$ is the angle between the relevant transition dipole moments of the interacting pigments (see Fig. 3). The angle $\phi_{12}$ depends on the orientation of the transition dipole moment within the molecular frame of the chlorophyll molecule. In Fig. 4 $A$ $r_{eqM}$ is plotted as a function of $\alpha$. The vertical dashed line shows the value of $r_{eqM}$ in the case where the transition dipole moments are not rotated ($\alpha$ is 90°, parallel to the $y$ axis). The horizontal dotted line shows the experimentally determined anisotropy after equilibration within the monomer, and the gray area reflects the error margin ($r_1 = 0.16 \pm 0.02$). Clearly, a value of $\alpha = 89-94°$ leads to a good correspondence between experiment and calculation. Other regions where the experimental and calculated anisotropy are in agreement are 9–15°, 57–63°, and 158–163°. However, we do not
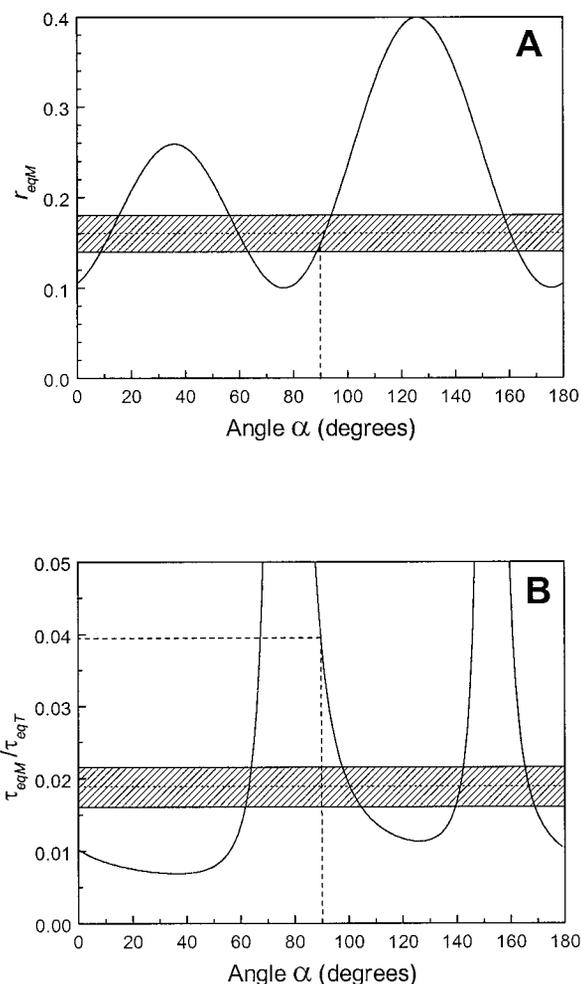
FIGURE 4 (*A*) The amplitude of the anisotropy "after" equilibration within the monomer ($r_{eqM}$) as a function of $\alpha$. The vertical dashed line indicates $r_{eqM}$ for $\alpha$ is 90° ($Q_y$ along the $y$ axis; see Fig. 3). The horizontal dotted line gives the experimentally determined value, and the gray area shows the error margin. (*B*) The calculated ratio $\tau_{eqM}/\tau_{eqT}$ as a function of the angle $\alpha$. The vertical dashed line indicates that the ratio for $\alpha$ is 90°. The horizontal dotted line gives the experimentally determined ratio, and the gray area shows the error margin.

expect that the transition dipole moment has an orientation differing that much from the $y$ axis, because in, e.g., BChl $a$ bound to protein, $\alpha$ is also close to 90°, as can be concluded from modeling studies on LH2 (Koolhaas et al., 1998) and the FMO complex (Louwe et al., 1997; Vulto et al., 1999).

Subsequently, the expected residual anisotropy in the case of trimers ($r_{eqT}$) for $\alpha = 89-94°$ can be calculated, assuming that in our sample all PCP is trimeric. A value ranging between 0.04 and 0.05 is found for $r_{eqT}$, which is lower than the experimentally determined residual anisotropy ($r_\infty = 0.11 \pm 0.02$). A similar, relatively high value was found in steady-state anisotropy measurements performed both at room temperature and 4 K (unpublished results). This shows that the assumption that the preparation

exclusively contains trimers is not correct. On the other hand, if the preparation would contain only monomers, we would not observe a slow depolarization time. Moreover, the linear dichroism spectrum would be completely different (Kleima, 1999). Obviously, the preparation consists of a mixture, which is in line with the results of the ultracentrifugation experiments (see above). For instance, assuming that 50% of the total amount of Chl $a$ is bound to trimers and 50% is bound to monomers would explain the experimental residual anisotropy. However, if trimers and monomers are present and the aggregation is not entirely cooperative, the presence of dimers cannot be excluded, although there are no biochemical indications that these indeed exist.

The ratio $\tau_1/\tau_2$ is the third experimental parameter that provides information about the energy transfer in PCP. This ratio is not influenced by the presence of monomers, although it is affected by the possible presence of dimers (see below). At first, we will neglect the possible fraction of dimers. In Fig. 4 $B$ the calculated ratio $\tau_{eqM}/\tau_{eqT}$ is shown as a function of $\alpha$. The asymptotes correspond to the case where $\kappa$ for the intramonomer equilibration rate becomes zero ($\tau_{eqM} \rightarrow \infty$). The value for $\kappa$ can be positive or negative, depending on the direction of the transition dipole moment; however, because the transfer rate is proportional to $\kappa^2$, the period is 180°. The dashed line shows the ratio $\tau_{eqM}/\tau_{eqT}$, which is 0.038 for unrotated transition dipole moments ($\alpha$ is 90°, parallel to the $y$ axis). The dotted line shows the average value for the experimentally determined ratio ($\tau_1/\tau_2 = 0.019 \pm 0.003$), and the gray area reflects the error margin. Correspondence between the experimentally determined and calculated values is found for $\alpha = 97$–$105°$. Other regions are 60–65°, 139–142°, and 164–169°. However, as discussed above, these values are not realistic.

The discussion in the preceding paragraphs concerning trimers (or monomers and trimers) is summarized in Fig. 5 $A$, where the amplitude of the anisotropy $r_{eqM}$ (*dashed, right y axis*), the residual anisotropy $r_{eqT}$ (*dotted, right y axis*), and the ratio $\tau_{eqM}/\tau_{eqT}$ (*solid, left y axis*) are shown for $\alpha$ ranging from 80° to 110°. The ranges of $\alpha$ values (represented by *gray areas*) corresponding to the experimental parameters $r_1$ and $\tau_1/\tau_2$ do not overlap. The highest value for $\alpha$ based on the experimentally determined value for $r_1$ is $\alpha = 94°$, whereas the lowest value for $\alpha$ based on $\tau_1/\tau_2$ is $\alpha = 97°$.

Alternatively, if we assume that the preparation contains only dimers (or dimers and monomers), which are organized like trimers missing one monomeric unit, we can define the residual anisotropy in the dimer ($r_{eqD}$) and the ratio $\tau_{eqM}/\tau_{eqD}$, where $\tau_{eqD}$ is the equilibration time constant within the dimer ($\tau_{eqD} = 1.5 \times \tau_{eqT}$). Fig. 5 $B$ is similar to Fig. 5 $A$, but represents the case of dimers. In this case there is horizontal overlap of the gray areas for $\alpha = 92$–$94°$. The residual anisotropy ranges from 0.075 to 0.09, which is in reasonable agreement with the measured residual anisotropy. It should be noted that trimers containing a Chl $a$ that does not
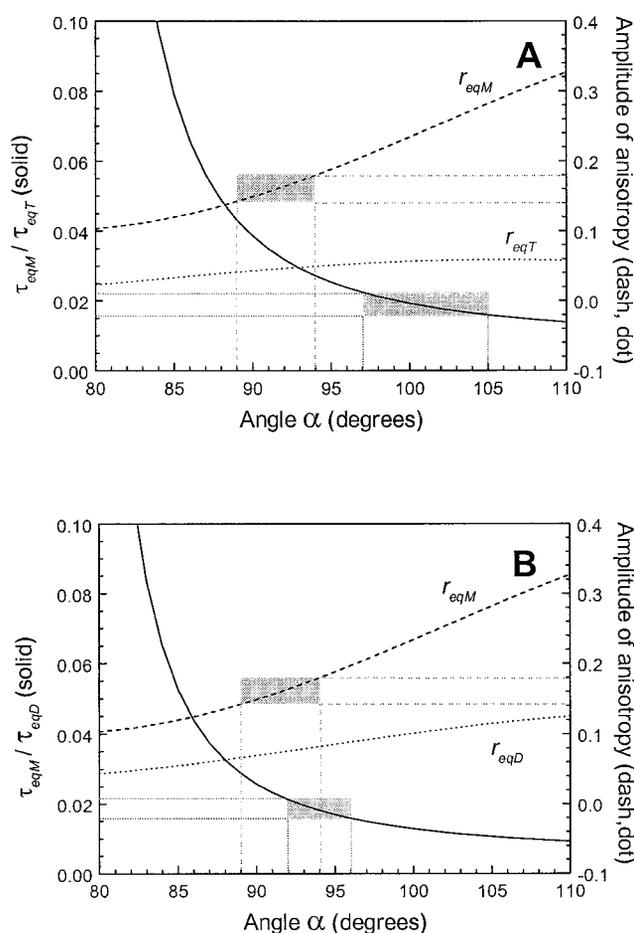


FIGURE 5 (*A*) The ratio $\tau_{eqM}/\tau_{eqT}$ (*solid, left y axis*) and the amplitude (*right y axis*) of the anisotropy "after" equilibration within the monomer ($r_{eqM}$, *dashed line*) and the residual anisotropy ($r_{eqT}$, *dotted line*) are plotted versus $\alpha$. The gray areas reflect the experimentally determined values of the ratio $\tau_1/\tau_2$ and the remaining anisotropy "after" equilibration within the monomer ($r_1$). (*B*) Same as in *A*, but in the case where the preparation consists of 100% dimers, $\tau_{eqD}$ reflects the time constant for equilibration within the dimer and $r_{eqD}$ reflects the residual anisotropy.

transfer properly will also show a depolarization behavior between those of dimers and trimers.

Summarizing, the data indicate that we do not have only monomers (or trimers), and the data can be explained by the exclusive presence of dimers, but this is in disagreement with biochemical experiments. We are probably dealing with a mixture of monomers, dimers, and trimers. Assuming dimers (or dimers and monomers) implies that $\alpha = 92°$–$94°$, the simultaneous presence of trimers tends to favor the slightly larger values of $\alpha$.

It has been concluded by van Zandvoort et al. (1995) that $\alpha$ differs for absorption and emission. This is, in principle, due to "solvent" relaxation, but it is demonstrated in Appendix 1 that for Förster transfer between isoenergetic pigments one cannot simply use different values for $\alpha$ in the case of absorption and emission, because this leads to a

conflict with the laws of thermodynamics. Nevertheless, in the event of transfer between isoenergetic pigments the value of $\alpha$ may in principle vary as a function of the absorption/emission wavelength. If the variation exists, then the values estimated above should be considered an effective (average) orientation.

## Estimation of the refractive index

In the previous paragraph we have estimated, using the experimentally determined values for the anisotropy $r_1$ and the ratio $\tau_1/\tau_2$, the values of $\alpha$ that lead to agreement between the experimental data and the calculations using the PCP structure. With this information about $\alpha$, the calculated time constants $\tau_{eqM}$ and $\tau_{eqT}$ (and/or $\tau_{eqD}$) can be scaled to "real" time constants, using the refractive index, $k_r^D$ and the overlap integral, together forming the constant part ($C$) of the Förster equation. In Appendix 2 this factor ($C$) is determined. The radiative lifetime is estimated from literature values for the fluorescence quantum yield and the fluorescence lifetime of Chl $a$ (Seely and Conolly, 1986), leading to $C = 42/n^4 \text{ ps}^{-1} \text{ nm}^6$ for $\tau_r^D = 18.5$ ns (for details see Appendix 2). The refractive index can be used for the actual scaling of the calculated time constants to "real" time constants.

In Table 1 the results are shown. We have examined the consequences for the refractive index for both scaling to $\tau_1$ (upper half of Table 1) and scaling to $\tau_2$ (lower half of Table 1). The first column shows whether we assume trimers (and monomers) or dimers (and monomers), the second column gives the upper and lower limits of $\alpha$ as determined in the previous paragraph, the third column gives the calculated ratio $\tau_1/\tau_2$ (for that particular $\alpha$ and the assumed composition of the preparation), and the fourth column gives the experimentally determined upper and lower values of $\tau_1$. The column with heading $\tau_2$ presents the time constants resulting from the values for the ratio and $\tau_1$ in the same row. In the next column the corresponding scaling factor is shown. The last column shows the resulting values for $n$. The lower part of Table 1 is the same as the upper part, but in this case $\tau_2$ represents the experimentally determined value.

Clearly, the refractive indices required for proper scaling of the time constants in the case where the preparation is assumed to consist of trimers (and monomers) are higher than those in the case of dimers (and monomers). The average refractive index is $1.6 \pm 0.1$, where the error margins reflect the standard deviation. This value is significantly higher than the refractive index of the medium, which is water in this case ($n = 1.33$). It was suggested by Moog et al. (1984) that the refractive index in the Förster equation should be interpreted as that of the bulk solution. Our data are clearly not in agreement with that statement, and the effect of the protein and/or the peridinins should be taken into account. By very different methods, the refractive

**TABLE 1 Scaling of the calculated equilibration time constants to the experimental time constants**

| Sample | $\alpha$ (°) | $\tau_1/\tau_2$ calculated | $\tau_1$ (ps) | $\tau_2$ (ps) | Scaling factor | $n$ |
|---|---|---|---|---|---|---|
| Scaling to $\tau_1$ | | | | | | |
| Trimer | 94 | 0.0272 | 6.0 | 221 | 8.148 | 1.51 |
| | | | 7.6 | 279 | 6.432 | 1.60 |
| | 97 | 0.0224 | 6.0 | 269 | 6.409 | 1.60 |
| | | | 7.6 | 339 | 5.060 | 1.70 |
| Dimer | 92 | 0.0212 | 6.0 | 283 | 9.925 | 1.43 |
| | | | 7.6 | 358 | 7.836 | 1.52 |
| | 94 | 0.0181 | 6.0 | 331 | 8.148 | 1.51 |
| | | | 7.6 | 420 | 6.432 | 1.60 |
| Scaling to $\tau_2$ | | | | | | |
| Trimer | 94 | 0.0272 | 9.1 | 335 | 5.370 | 1.67 |
| | | | 9.9 | 365 | 4.928 | 1.71 |
| | 97 | 0.0224 | 7.5 | 335 | 5.122 | 1.69 |
| | | | 8.2 | 365 | 4.701 | 1.72 |
| Dimer | 92 | 0.0212 | 7.1 | 335 | 8.371 | 1.50 |
| | | | 7.7 | 365 | 7.683 | 1.53 |
| | 94 | 0.0181 | 6.1 | 335 | 8.055 | 1.51 |
| | | | 6.6 | 365 | 7.393 | 1.54 |
| Average $n$ | | | | | | $1.6 \pm 0.1$ |

Scaling is based on the value of the first intramonomer equilibration time $\tau_1$ (*upper part*) or on the slow intermonomer equilibration time $\tau_2$ (*lower part*). The first column shows whether trimers (and monomers) or dimers (and monomers) are assumed. The second column gives the upper and lower limits of $\alpha$, the third column gives the calculated ratio $\tau_1/\tau_2$ (for that particular $\alpha$ and the assumed composition of the preparation), and the fourth column gives the experimentally determined upper and lower values of $\tau_1$. The column with the heading $\tau_2$ shows the time constants resulting from the values for the ratio and $\tau_1$ in the same row. The next column shows the corresponding scaling factor. The last column shows the values for $n$ (using $C = 42/n^4 \text{ ps}^{-1} \text{ nm}^6$).

indices of, for example, LH2 and CP47 have been determined to be 1.63 (Andersson et al., 1991) and 1.51 (Renge et al., 1996), respectively.

To illustrate the dependence of the transfer rates between individual pigments (numbering according to Fig. 3) on the value of $\alpha$, these rates are shown in Table 2 for $\alpha = 92°$ and for $\alpha = 97°$, using $C = 42/n^6 \text{ ps}^{-1} \text{ nm}^6$ and the average value of $n$ (= 1.6). In addition, the corresponding factors $\kappa^2/R^6$ and the time constants are shown. The equilibration time constant in the case of dimers with $\alpha = 92°$ is 438 ps, whereas in the case of trimers with $\alpha = 97°$ we find 269 ps. Note that the discrepancy with the experimental value is due to the strong dependence of the transfer rates on $n$ (see Table 1).

We have shown here that the Chl $a$ to Chl $a$ excitation energy transfer in PCP can very well be modeled using the Förster equation. The crystal structure, in which the molecular frames of the Chl $a$ molecules were resolved, enabled us to estimate the orientation of the $Q_y$ transition dipole moments and conclude that $\alpha = 94.5 \pm 2.5°$. By using this value of $\alpha$, the experimentally determined excitation equilibration time constants of $6.8 \pm 0.8$ ps and $350 \pm 15$ ps can be assigned to equilibration times within the monomer and within the trimer/dimer, respectively.

**TABLE 2   Calculated rates and time constants for transfer between individual pigments in PCP**

| Pigments #,# | $\kappa^2/R^6$ (nm$^{-6}$) | $k$ (ps$^{-1}$) | $\tau$ |
|---|---|---|---|
| $\alpha = 92°$ | | | |
| 1,2 | $8.396*10^{-3}$ | 0.054 | 18.6 ps |
| 1,3 | $6.278*10^{-5}$ | $4.023*10^{-4}$ | 2.49 ns |
| 1,4 | $2.222*10^{-4}$ | $1.424*10^{-3}$ | 0.70 ns |
| 2,3 | $1.054*10^{-5}$ | $6.755*10^{-5}$ | 14.8 ns |
| 2,4 | $6.107*10^{-5}$ | $3.914*10^{-4}$ | 2.56 ns |
| | | | |
| $\alpha = 97°$ | | | |
| 1,2 | 0.013 | 0.083 | 12 ps |
| 1,3 | $7.061*10^{-5}$ | $4.525*10^{-4}$ | 2.21 ns |
| 1,4 | $2.539*10^{-4}$ | $1.627*10^{-3}$ | 0.61 ns |
| 2,3 | $1.533*10^{-5}$ | $9.823*10^{-5}$ | 10.2 ns |
| 2,4 | $4.875*10^{-5}$ | $3.124*10^{-4}$ | 3.20 ns |

The calculated factors $\kappa^2/R^6$, the transfer rates, and the transfer times are shown for $\alpha = 92°$ and for $\alpha = 97°$. Pigments are numbered as indicated in Fig. 3. A refractive index of 1.6 was used, and $C$ was $42/n^4$ ps$^{-1}$ nm$^6$.

## What can be said about the in vivo functioning of PCP?

Because of the relatively slow energy transfer from one monomer to the next within the PCP complex, one could wonder whether this transfer will actually occur in vivo, because other transfer processes might be faster. When two trimeric PCP complexes are oriented favorably with respect to each other, PCP-to-PCP transfer can be faster than the intermonomeric transfer within one trimeric complex (Hofmann, manuscript in preparation). However, it is not very likely that larger in vivo aggregates of PCP complexes are formed, as suggested by Knoetzel and Rensing (1990), because such aggregates have not been isolated and are not formed upon crystallization. The probably more important energy transfer processes that might compete with those within the PCP complex are the transfer processes to the membrane-bound PSII complex. However, it is not known whether this transfer occurs via the LHC$a/c$ complex (Hofmann et al., 1996), via the CP43 or CP47 complexes (Mimuro et al., 1990), or directly to the PSII core complex (Knoetzel and Rensing, 1990). Because the LHC$a/c$ complex is to some extent similar to the LHCII complex of green plants (Hiller et al., 1995), it might be modeled on the basis of the crystal structure of LHCII (Kühlbrandt et al., 1994; Hofmann, unpublished results), and therefore it forms the "easiest" candidate for some tentative calculations. The PCP $\rightarrow$ LHC$a/c$ transfer can be calculated by using this model, the assignment of Chl $a$ according to Kühlbrandt et al. (1994), and the orientations of transition dipole moments according to Gradinaru et al. (1998), $n = 1.6$ and $C = 42/n^6$. If the trimer axis of PCP and LHC$a/c$ are aligned, the orientation (in terms of rotation along the trimer axis) is as favorable as possible, PCP and LHC$a/c$ are as close as possible, and PCP is located on the luminal side, the shortest transfer time from a PCP Chl $a$ to a LHC$a/c$ Chl $a$ is ~140

ps (Hofmann, manuscript in preparation). This is shorter than the transfer time between two PCP monomers (~1 ns). Including the (unfavorable) transfer from the other Chl $a$ in the PCP monomer and the transfer to other LHC$a/c$ Chl $a$ molecules, an average transfer time of ~150 ps is found in this specific case. We thus might speculate that some transfer to the LHC$a/c$ complex competes with transfer between monomers, although it should be emphasized that the numbers given here strongly depend on the modeling parameters.

## APPENDIX 1: ROTATION OF TRANSITION DIPOLE MOMENTS

It was concluded from angle-resolved fluorescence depolarization experiments on Chl $a$ oriented in nitrocellulose film that the transition dipole moments for absorption and emission are not oriented parallel to each other, but are at an angle of 17–19° with respect to each other (van Zandvoort et al., 1995). The transition dipole moment for absorption was found to be parallel to the $Q_y$ axis ($\alpha = 90°$) of the Chl molecule, while the transition dipole moment for emission is oriented at $\alpha$ is 107–109° in the plane of the Chl molecule (see *inset* of Fig. 3). The time scale of this rotation could easily be on the order of a few picoseconds because it might be related to solvent (protein) relaxation processes that have been shown to occur on such time scales in the case of Chl $b$ (Oksanen et al., 1998) and therefore could be of importance in photosynthetic complexes. Below we will examine the consequences for Förster excitation energy transfer.

In Fig. 6 three imaginary photosynthetic complexes are shown. The pigments are isoenergetic, and the transition dipole moments of each pigment for absorption and emission are, respectively, $\mu_A$ and $\mu_E$. In Fig. 6 $A$ two pigments are placed at rotationally symmetrical positions with respect to the axis perpendicular to the plane of the paper. For excitation energy transfer from pigment 1 to 2 the transition dipole moments $\mu_{1E}$ and $\mu_{2A}$ are involved, while for transfer from 2 to 1 $\mu_{2E}$ and $\mu_{1A}$ are involved. Because of the symmetrical position of the pigments with respect to each other, $\kappa^2_{1\rightarrow2}$ equals $\kappa^2_{2\rightarrow1}$, so that back and forward excitation energy transfer rates are the same. In Fig. 6 $B$ an asymmetrical dimer is shown. Because in this case the angle between $\mu_{3E}$ and $\mu_{4A}$ is not the same as the angle between $\mu_{4E}$ and $\mu_{3A}$, it follows that $\kappa^2_{3\rightarrow4}$ is not equal to $\kappa^2_{4\rightarrow3}$. Therefore, in equilibrium relatively more excitations would be located on pigment 3 than on pigment 4, although the pigments are isoenergetic. In Fig. 6 $C$ a symmetrical trimeric structure is shown. In the trimer the pigments 5 and 6 are at the same positions with respect to each other as the pigments 3 and 4. As a consequence, the transfer from pigment 6 to 5 is faster than that from pigment 5 to 6, and the same holds for the pigment pairs 5–7 and 7–6. In other words, in the case of three isoenergetic pigments with different orientations of the transition dipole moments for absorption and emission, the excitation would continuously circle around, which seems counterintuitive.

In the case of isoenergetic pigments in the asymmetrical dimer, the unidirectionality of transfer is thermodynamically impossible. Apparently, rotation of the transition dipole moment in the excited state cannot occur without affecting the energy of the excited state. In other words, it is no longer correct to assume that the energy of the pigment in the excited state and the orientation of the transition dipole moment are independent properties. An explanation for this feature is that the rotation of the transition dipole moment might be caused by solvent reorganization effects, in general leading to a lowering of the energy of the excited state. Förster excitation energy transfer only takes place when the corresponding instantaneous donor and acceptor transition energies are the same. As a consequence, formally the orientation factor in the Förster equation becomes
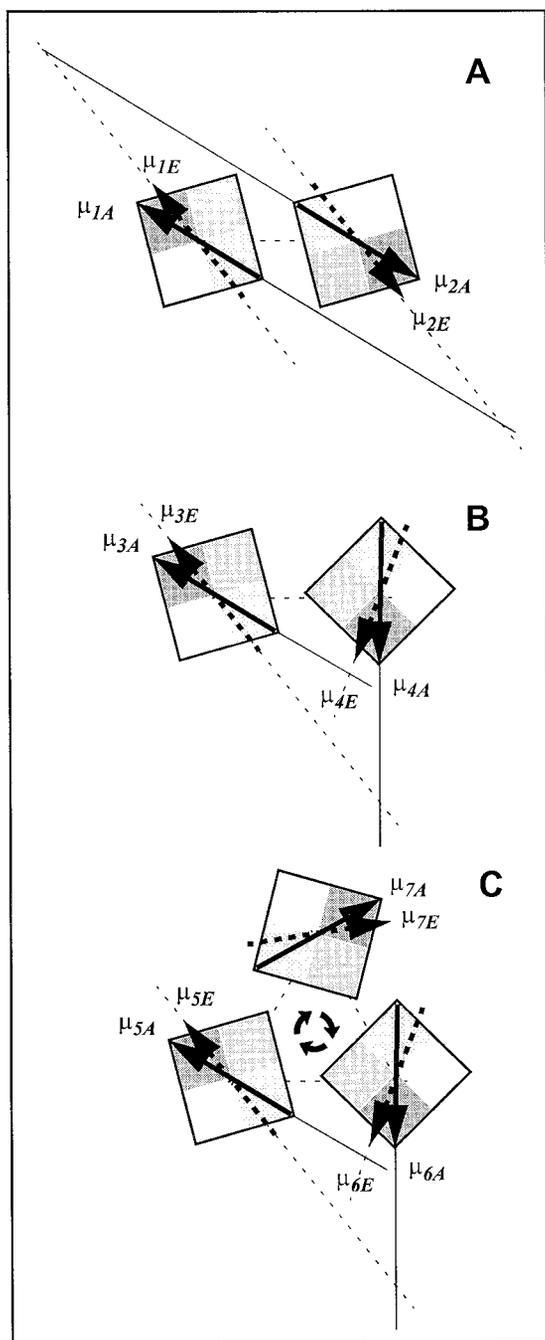
FIGURE 6 Effect of the orientation of transition dipole moments for absorption ($\mu_A$) and emission ($\mu_E$) on the orientation factor ($\kappa$) for three imaginary configurations. Shown are a rotational symmetrical dimer (*A*), an asymmetrical dimer (*B*), and a trimer (*C*). Squares reflect Chl *a*, with the plane of the molecule parallel to the plane of the paper.

energy dependent and therefore has to be included in the overlap integral:

$$k_{DA} = 8.8 \times 10^{17} \cdot \frac{k_r^D}{R^6 n^4} \cdot \int \kappa^2(\tilde{\nu}) \frac{\epsilon_A(\tilde{\nu}) f_D(\tilde{\nu})}{\tilde{\nu}^4} d\tilde{\nu}$$

In conclusion, when one allows different orientations of the transition dipole moments for absorption and emission, one should evaluate the above expression. In the case of PCP we have considered the situation where the transition dipole moments for absorption and emission are parallel, but we have rotated the transition dipole moment over an angle $\alpha$ with respect to the molecular frame. The value for $\alpha$ is taken to be the same for all pigments. Thus the angle should be considered as an effective "average" angle.

## APPENDIX 2

Below the constant factor in the Förster equation, consisting of the overlap integral and the radiative rate, is calculated.

To calculate the overlap integral in the Förster equation, the extinction coefficient of PCP in the Chl *a* $Q_y$ band has to be estimated. To that end the absorption spectrum of the $Q_y$ band in PCP has been compared to that of Chl *a* in different solvents with known extinction coefficients. The FWHM of the $Q_y$ band in the OD spectrum of PCP is 14 nm (see Fig. 1). The extinction coefficients and FWHMs of the $Q_y$ band of Chl *a* are 90.25 mM$^{-1}$ cm$^{-1}$ in ether (FWHM 17 nm; Lichtenthaler, 1987), 79.6 mM$^{-1}$ cm$^{-1}$ in 100% methanol (FWHM 22 nm; Eijckelhoff and Dekker, 1995), and 86 mM$^{-1}$ cm$^{-1}$ in aqueous acetone (FWHM 20 nm; Eijckelhoff and Dekker, 1995) (Lichtenthaler, 1987; Porra et al., 1989). Assuming that the dipole strengths of Chl *a* in PCP and in these solvents are the same, we have normalized the areas of the absorption spectra with respect to each other in the $Q_y$ region and thus estimated the extinction coefficient of Chl *a* in PCP to be ~110 mM$^{-1}$ cm$^{-1}$.

The radiative rate in the Förster equation is estimated by using $k_r^D = \phi_f/\tau_f$, where $\tau_f$ is the fluorescence lifetime and $\phi_f$ is the quantum yield for fluorescence. Using literature values for $\tau_f$ and $\phi_f$ for Chl *a* in methanol and in ether, we find an average radiative lifetime of 18.5 ns (Seely and Conolly, 1986). So for *C* we find a value of $42/n^4$ ps$^{-1}$ nm$^6$.

## REFERENCES

Akimoto, S., S. Takaichi, T. Ogata, Y. Nishimura, I. Yamazaki, and M. Mimuro. 1996. Excitation energy transfer in carotenoid-chlorophyll protein complexes probed by femtosecond fluorescence decays. *Chem. Phys. Lett.* 190:147–152.

Andersson et al. 1991. Absorption spectral shifts of carotenoids related to medium polarizability. *Photochem. Photobiol.* 54:353–360.

Bautista, J. A., K. Atticks, R. G. Hiller, F. P. Sharples, D. Gosztola, M. Wasielewski, and H. Frank. 1999. Singlet and triplet energy transfer in the peridinin-chlorophyll-*a*-protein from *Amphedinium carterae*. *J. Phys. Chem. A.* 103:2267–2273.

Cantor, C. R., and P. R. Schimmel. 1980. Biophysical Chemistry, Part II, Techniques for the Study of Biological Structure and Function. W. H. Freeman, New York.

Carbonera, D., and G. Giacometti. 1995. FDMR spectroscopy of peridinin-chlorophyll-a protein from *Amphidinium carterae. Spectrochim. Acta.* 51A:115–123.

Carbonera, D., G. Giacometti, and U. Serge. 1996. Carotenoid interactions in peridinin chlorophyll a protein from dinoflagellates. *J. Chem. Soc. Faraday Trans.* 92:989–993.

Causgrove, T. P., S. Yang, and W. S. Struve. 1988. Polarized pump-probe spectroscopy of exciton transport in bacteriochlorophyll a-protein from *Phosthecochloris aestuarii. J. Phys. Chem.* 92:6790–6795.

Debreczeny, M. P., K. Sauer, J. Zhou, and D. Bryant. 1993. Monomeric C-Phycocyanin at room temperature and 77K: resolution of the absorp-

tion and fluorescence spectra of the individual chromophores and the energy transfer rate constants. *J. Phys. Chem.* 97:9852–9862.

Debreczeny, M. P., K. Sauer, J. Zhou, and D. Bryant. 1995a. Comparison of calculated and experimentally resolved rate constants for excitation energy transfer in C-phycocyanin. 1. Monomers. *J. Phys. Chem.* 99: 8412–8419.

Debreczeny, M. P., K. Sauer, J. Zhou, and D. Bryant. 1995b. Comparison of calculated and experimentally resolved rate constants for excitation energy transfer in C-phycocyanin. 2. Trimers. *J. Phys. Chem.* 99: 8420–8431.

Duerring, M., G. B. Schmidt, and R. Huber. 1991. Isolation, crystallization, crystal structure analysis and refinement of the constitutive C-phycocyanin from the chromatically adapting cyanobacterium *Fremyella diplosiphon* at 1.66 Å resolution. *J. Mol. Biol.* 217:577–592.

Eijckelhoff, C., and J. P. Dekker. 1995. Determination of the pigment stoichiometry of the photochemical reaction center of photosystem II. *Biochim. Biophys. Acta.* 1231:21–28.

Förster, Th. 1965. *In* Modern Quantum Chemistry, Part II. O. Sinanoglu, editor. Academic Press, New York. 93–137.

Gillbro, T., A. V. Sharkov, I. V. Kryukov, E. V. Khoroshilov, P. G. Kryukov, R. Fisher, and H. Scheer. 1993. Förster excitation energy transfer between neighbouring chromophores in C-phycocyanin trimers. *Biochim. Biophys. Acta.* 1140:321–326.

Gradinaru, C. C., S. Özdemir, D. Gülen, I. van Stokkum, R. van Grondelle, and H. van Amerongen. 1998. The flow of excitation energy in LHCII monomers: implications for the structural model of the major plant antenna. *Biophys. J.* 75:3064–3077.

Hiller, R. G., P. M. Wrench, and F. P. Sharples. 1995. Amino acid sequences of the light-harvesting proteins of the dinoflagellate *Amphidinium carterae. In* Photosynthesis: From Light to Biosphere, Vol. 1. P. Mathis, editor. Kluwer, Dordrecht, the Netherlands. 29–34.

Hofmann, E., P. Wrench, F. P. Sharples, R. G. Hiller, W. Welte, and K. Diedrichs. 1996. Structural basis of light harvesting by carotenoids: peridinin-chlorophyll-protein from *Amphidinium carterae. Science.* 272: 1778–1791.

Kleima, F. J. 1999. Light-harvesting and excitation energy transfer in oxygenic photosynthesis. Ph.D. thesis. Vrije Universiteit, Amsterdam.

Knoetzel, J., and L. Rensing. 1990. Characterization of the photosynthetic apparatus from the marine dinoflagellate *Gonyaulax polyedra*. I. Pigment and polypeptide composition of the pigment protein complexes. *J. Plant Physiol.* 136:271–279.

Koka, P., and P.-S. Song. 1977. The chromophore topography and binding environment of peridinin chlorophyll-a-protein complexes from marine dinoflagellate algae. *Biochim. Biophys. Acta.* 495:220–231.

Koolhaas, M. H. C., R. N. Frese, G. J. S. Fowler, T. A. Bibby, S. Georgakopoulou, G. van der Zwan, C. N. Hunter, and R. van Grondelle. 1998. Identification of the upper exciton component of the B850 bacteriochlorophylls of the LH2 antenna complex, using a B800-free mutant of *Rhodobacter sphearoides. Biochemistry.* 37:4693–4698.

Kühlbrandt, W., D. N. Wang, and Y. Fujioshi. 1994. Atomic model of the plant light-harvesting complex by electron crystallography. *Nature.* 367: 614–621.

Lichenthaler, H. K. 1987. Chlorophylls and carotenoids: pigments of photosynthetic biomembranes. *Methods Enzymol.* 148:350–382.

Louwe, R. J. W., J. Vrieze, A. J. Hoff, and T. J. Aartsma. 1997. Toward an integral interpretation of the optical steady-state spectra of the FMO complex of *Prosthecochloris aestuarii*. 2. Exciton simulations. *J. Phys. Chem. B.* 101:11280–11287.

Mimuro, M., N. Tamai, T. Ishimaru, and I. Yamazaki. 1990. Characteristic fluorescence components in the photosynthetic pigment system of a marine dinoflagellate, *Protogonyaulax tamarensis*, and the excitation flow among them. Studies by means of steady-state and time-resolved fluorescence spectroscopy. *Biochim. Biophys. Acta.* 1016:280–287.

Moog, S. R., A. Kuki, M. D. Fayer, and G. Boxer. 1984. Excitation transport and trapping in a synthetic chlorophyllide substituted hemoglobin: orientation of the chlorophyll $S_1$ transition dipole. *Biochemistry.* 23:1564–1571.

Oksanen, J. A. I., P. Martinsson, E. Åkesson, P. H. Hynninen, and V. Sundström. 1998. Transient hole burning and solvatation dynamics of chlorophyll *b* monomers in various solvent environments. *J. Phys. Chem. A.* 102:4328–4336.

Porra, R. J., W. A. Thomson, and P. E. Kriedemann. 1989. Determination of accurate extinction coefficients and simultaneous equations for assaying chlorophylls *a* and *b* extracted with four different solvents: verification of the concentration of chlorophyll standards by atomic absorption spectroscopy. *Biochim. Biophys. Acta.* 975:384–384.

Renge, I., R. van Grondelle, and J. P. Dekker. 1996. Matrix and temperature effects on the absorption spectra of $\beta$-carotene and pheophytin *a* in solution and in green plant photosystem II. *J. Photochem. Photobiol.* 96:109–121.

Schirmer, T., W. Bode, and R. Huber. 1987. Refined three dimensional structures of two cyanobacterial C-phycocyanins at 2.1 and 2.5 Å resolution. *J. Mol. Biol.* 196:677–695.

Seely, G. R., and J. S. Conolly. 1986. Fluorescence of photosynthetic pigments in vitro. *In* Light Emission by Plants and Bacteria. Govindjee, J. Amesz, and D. C. Fork, editors. Academic Press, Orlando. 99–133.

Song, P.-S., P. Koka, B. B. Prézelin, and T. Haxo. 1976. Molecular topology of the photosynthetic light-harvesting complex peridinin-chlorophyll-a-protein, from marine dinoflagellates. *Biochemistry.* 15: 4422–4427.

van Stokkum, I. H. M., T. Scherer, A. M. Brouwer, and J. W. Verhoeven. 1994. Conformational dynamics of flexibly and semi-rigidly bridged donor-acceptor systems as revealed by spectrotemporal parameterization of fluorescence. *J. Phys. Chem.* 98:852–866.

van Zandvoort, M. A. M. J., D. Wrobel, P. Lettinga, G. van Ginkel, and Y. K. Levine. 1995. The orientation of the transition dipole moments of chlorophyll a and pheophytin a in their molecular frame. *Photochem. Photobiol.* 62:299–308.

Vulto, S. I. E., M. A. de Baat, R. J. W. Louwe, H. P. Permentier, T. Neef, M. Miller, H. van Amerongen, and T. J. Aartsma. 1999. Exciton simulations of optical spectra of the FMO complex from the green sulfur bacterium chlorobium tepidum at 6K. *J. Phys. Chem. B.* 102:9577–9582.